

# Bifurcation analysis of the problem of a “rubber” ellipsoid of revolution rolling on a plane

A. A.Kilin, E. N.Pivovarova

Ural Mathematical Center,

Udmurt State University,

ul. Universitetskaya 1, Izhevsk, 426034 Russia

## Abstract

This paper is concerned with the problem of an ellipsoid of revolution rolling on a horizontal plane under the assumption that there is no slipping at the point of contact and no spinning about the vertical. A reduction of the equations of motion to a fixed level set of first integrals is performed. Permanent rotations corresponding to the rolling of an ellipsoid in a circle or in a straight line are found. A linear stability analysis of permanent rotations is carried out. A complete classification of possible trajectories of the reduced system is performed using a bifurcation analysis. A classification of the trajectories of the center of mass of the ellipsoid depending on parameter values and initial conditions is performed.

## Contents

<b>1</b>	<b>Introduction</b>	<b>2</b>
<b>2</b>	<b>Equations of motion for a body of revolution on a plane</b>	<b>4</b>
2.1	Configuration space and kinematic relations . . . . .	4
2.2	Constraint equations and dynamical equations . . . . .	5
2.3	Invariants and symmetries . . . . .	7
2.4	Reduction to a system with one degree of freedom . . . . .	8
<b>3</b>	<b>Explicit form of the equations of motion for an ellipsoid of revolution</b>	<b>9</b>

<b>4</b>	<b>Bifurcation analysis</b>	<b>11</b>
4.1	General definitions . . . . .	11
4.2	Critical sets . . . . .	12
4.3	Example of a bifurcation diagram . . . . .	17
4.4	Bifurcations of critical sets and types of bifurcation diagrams	20
<b>5</b>	<b>Analysis of the trajectories of an ellipsoid</b>	<b>29</b>

# 1 Introduction

Analysis of the motion of rigid bodies on a plane is one of the classical problems in mechanics. To describe the motion of a rigid body in the first approximation, use is often made of conservative models: the model of an absolutely smooth plane (the point of contact can slip) and the model of an absolutely rough plane (the classical nonholonomic model in which there is no slipping at the point of contact). Another conservative model of contact is that of a rolling “rubber” body — it assumes that there is no slipping at the point of contact and no spinning about the vertical. Early studies of the rolling motion of bodies without spinning go back to the classical works on modern mechanics: this model was proposed by Hadamard [1] and developed by Beghin [2]. In [3], the term “rubber rolling” was introduced to describe this motion model. A systematization of results on the rolling motion of rigid bodies using the above-mentioned model was presented in [4, 5], where existing tensor invariants of the system depending on the shape of the body and the mass distribution in it were found.

The main feature of the problem of a body of revolution moving on a plane is its integrability regardless of the shape of the body. The same holds true for an absolutely smooth plane [6, 7], for an absolutely rough plane [8], and for the rubber body rolling model [4]. Moreover, if the system is subject to one nonholonomic constraint which prohibits sliding in the direction of the projection of the axis of rotation, then such a problem is also integrable. This was shown in [9], where the authors addressed the problem of the rolling motion of a sphere with axisymmetric mass distribution. It was shown that this system admits a redundant set of first integrals and an invariant measure, and that one of the found integrals is similar to the additional integral found in [10] in the problem of a circular disk rolling on smooth ice. This allowed a reduction to a system with one degree of freedom and made it possible to show that all nonsingular trajectories are periodic functions of time. It is interesting that, if the system is subject to a constraint prohibiting sliding in the direction perpendicular to the axis of

rotation, then the problem becomes nonintegrable [11]. For the case of the sphere with axisymmetric mass distribution it is shown that, in the general case, this system is nonintegrable (one additional integral of motion and an invariant measure are needed for the system to be integrable). It is numerically shown that the system exhibits chaotic dynamics. In addition, the problem of a body of revolution rolling on a plane remains integrable after adding an additional potential that is invariant under rotation about the vertical [12–14].

There is a related problem, that of a homogeneous sphere rolling without slipping on a surface of revolution, which is similar to the problem of a body of revolution rolling on a plane. This problem is also integrable regardless of the form of the surface. This is shown in [15, 16] using the same methods of analysis (in particular, reduction by symmetries). In [17, 18] the rolling motion of a sphere on an arbitrary rotating surface of revolution is investigated, and the authors of [19, 20] examine integrable cases of this problem: the rolling motions of a sphere on the rotating surface of a cone and a circular cylinder. In [21, 22] a new interesting problem concerning the rolling of spheres between two spherical surfaces is addressed and cases of its integrability are found, and in [23] the integrability of the related problem of the motion of a rigid body in a spherical suspension is shown [24].

Compared to the study of body motion using the classical nonholonomic model prohibiting only slipping at the point of contact, much less attention has been given in the literature to the dynamics of bodies using the rubber body model. In particular, analysis of rigid body dynamics using this model was made in [3, 25–27]. In [28], the rubber body model was employed to examine the dynamics of an unbalanced disk. The rolling motion of spheres with different mass distributions was studied in [3, 25–27, 29–33], and the motion of a triaxial ellipsoid was examined in [34].

However, the “rubber” motion model is applied not only in handling some model problems concerning, e.g., disks or spheres, but also in simulating the motion of mobile robots. In particular, the problem of using various motion models for simulating the dynamics of mobile robots is discussed in [35], where it is noted that the rolling motion of a sphere without slipping or spinning is the classical ball-plate problem [36, 37]. In [35], the authors also note that in many studies the vertical component of the angular velocity of the spherical robot is assumed to be zero since the possibility of omnidirectional motion allows motion control without using vertical rotations. Such a motion model is used in analyzing the dynamics of a spherical robot with a pendulum drive [38, 39], a spherical robot with an internal

platform [40, 41], a spherical robot with internal omniwheels [42, 43], and a spherical robot actuated by changing the gyrostatic momentum [44]. In addition, some authors [41, 42, 45, 46], who use the “rubber” motion model consider only kinematics without taking into account the system dynamics.

In this paper, we carry out a qualitative analysis of the motion of an ellipsoid of revolution on a horizontal plane using the model of rubber body. Although we restrict our attention to a special case of body shape, many conclusions of this paper will be valid for a body of an arbitrary shape as well. In addition, the analysis of the dynamics in specific problems remains of interest to researchers (see, e.g., the recent paper on qualitative analysis of the rolling motion of a torus on a plane [47]).

The paper is organized as follows. Section 2.1 presents equations of motion, invariants, and a reduction to a system with one degree of freedom for a body of revolution of arbitrary form. In Section 3, an explicit form of the equations of motion for an ellipsoid of revolution is presented. Section 4 provides a qualitative analysis of the dynamics of the ellipsoid and a complete classification of motions depending on parameters and values of first integrals. In Section 5, an analysis of the trajectories of the center of mass of the ellipsoid in absolute space is made and conclusions concerning the boundedness and unboundedness of the trajectories are drawn.

## 2 Equations of motion for a body of revolution on a plane

### 2.1 Configuration space and kinematic relations

Consider the rolling motion of a dynamically symmetric rigid body of revolution of mass  $m$  on an absolutely rough horizontal plane (Fig. 1). We will assume that the body rolls without slipping (the velocity of the point of contact is zero) and without spinning (the projection of the angular velocity of the body onto the vertical is zero), and has only one point of contact,  $P$ , with the supporting plane.

We introduce two coordinate systems:

- a fixed (inertial) coordinate system  $Oxyz$  with unit vectors  $\alpha, \beta, \gamma$ , where  $\gamma$  is a vertical unit vector;
- a moving coordinate system  $Cx_1x_2x_3$  with vectors  $e_1, e_2, e_3$  rigidly attached to the body, and with origin at its center of mass,  $C$ , such that the axis  $Cx_3$  is directed along the symmetry axis.

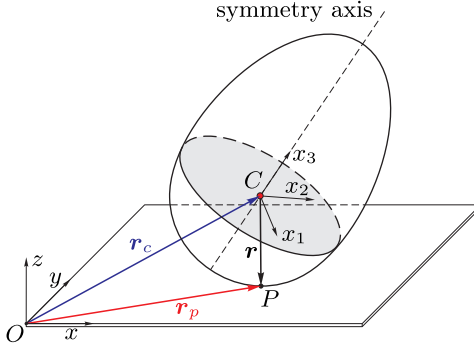


Figure 1: A body of revolution on a plane.

We will specify the position of the body of revolution by the coordinates of its center of mass  $\mathbf{r}_c = (x_c, y_c, z_c) \in \mathbb{R}^3$  in the coordinate system  $Oxyz$ , and its orientation in space, by the orthogonal matrix  $\mathbf{Q}$ , whose columns are the projections of the unit vectors  $\boldsymbol{\alpha}, \boldsymbol{\beta}, \boldsymbol{\gamma}$  onto the axes of the moving coordinate system  $Cx_1x_2x_3$

$$\mathbf{Q} = \begin{pmatrix} \alpha_1 & \beta_1 & \gamma_1 \\ \alpha_2 & \beta_2 & \gamma_2 \\ \alpha_3 & \beta_3 & \gamma_3 \end{pmatrix} \in SO(3).$$

Hence, the configuration space of the problem of the free motion of the body of revolution is the product  $\mathcal{N} = \{(\mathbf{r}_c, \mathbf{Q})\} = \mathbb{R}^3 \times SO(3)$ .

To describe the dynamics of the body on a plane, we introduce the vector of the angular velocity  $\boldsymbol{\omega} = (\omega_1, \omega_2, \omega_3)$  and the vector of the velocity of the center of mass  $\mathbf{v} = (v_1, v_2, v_3)$  and refer them to the moving coordinate system  $Cx_1x_2x_3$ <sup>1</sup>. Using these velocities (quasi-velocities), the evolution of the vector  $\mathbf{r}_c$  and the matrix  $\mathbf{Q}$  can be written as the kinematic relations

$$\begin{aligned} \dot{\boldsymbol{\alpha}} &= \boldsymbol{\alpha} \times \boldsymbol{\omega}, & \dot{\boldsymbol{\beta}} &= \boldsymbol{\beta} \times \boldsymbol{\omega}, & \dot{\boldsymbol{\gamma}} &= \boldsymbol{\gamma} \times \boldsymbol{\omega}, \\ \dot{\mathbf{r}}_c &= \mathbf{Q}^\top \mathbf{v}. \end{aligned} \tag{1}$$

## 2.2 Constraint equations and dynamical equations

We assume that the body rolls without loss of contact with the plane. This assumption implies that the following holonomic constraint is imposed on

<sup>1</sup>Here and below, unless otherwise specified, all vectors will be referred to the moving coordinate system  $Cx_1x_2x_3$ .

the system:

$$z_c + (\mathbf{r}, \boldsymbol{\gamma}) = 0, \quad (2)$$

where  $\mathbf{r}$  is the radius vector of the point of contact (see Fig. 1), which can be expressed in terms of the components of the vector  $\boldsymbol{\gamma}$ . Here and in what follows, by  $(\cdot, \cdot)$  we denote the scalar product. In the case of an arbitrary axisymmetric surface of the body, the dependence  $\mathbf{r}(\boldsymbol{\gamma})$  can be represented as

$$\mathbf{r}(\boldsymbol{\gamma}) = (\chi_1(\gamma_3)\gamma_1, \chi_1(\gamma_3)\gamma_2, \chi_2(\gamma_3)),$$

where  $\chi_1(\gamma_3)$  and  $\chi_2(\gamma_3)$  are arbitrary functions related to each other by [14]

$$\frac{d\chi_2}{d\gamma_3} = \chi_1 - \frac{1 - \gamma_3^2}{\gamma_3} \frac{d\chi_1}{d\gamma_3}.$$

This relation is obtained from the condition  $(\dot{\mathbf{r}}, \boldsymbol{\gamma}) = 0$ .

The no slip condition at the point of contact is described by a constraint of the form

$$\mathbf{f} = \mathbf{v} + \boldsymbol{\omega} \times \mathbf{r} = \mathbf{0}. \quad (3)$$

*Remark.* Two projections of equation (3),  $(\mathbf{f}, \boldsymbol{\alpha})$  and  $(\mathbf{f}, \boldsymbol{\beta})$ , are nonholonomic constraints, and the third,  $(\mathbf{f}, \boldsymbol{\gamma})$ , is the time derivative of equation (2).

The condition that there be no spinning about the vertical is described by another nonholonomic constraint:

$$g = (\boldsymbol{\omega}, \boldsymbol{\gamma}) = 0. \quad (4)$$

The kinetic energy  $T$  and the potential energy  $U$  of the system have the form

$$T = \frac{1}{2}(\boldsymbol{\omega}, \mathbf{I}\boldsymbol{\omega}) + \frac{1}{2}m(\mathbf{v}, \mathbf{v}), \quad U = -mg(\mathbf{r}, \boldsymbol{\gamma}),$$

where  $\mathbf{I} = \text{diag}(i_1, i_1, i_3)$  is the principal central tensor of inertia of the body and  $g$  is the free-fall acceleration.

*Remark.* Note that, due to the axial symmetry, the potential energy  $U$  of the system depends only on the inclination of the symmetry axis relative to the vertical, that is, the component  $\gamma_3$ .

We write the equations of motion of the system in the absence of external forces as Lagrange equations in quasi-velocities with constraints [48, 49]

$$\begin{aligned} \frac{d}{dt} \left( \frac{\partial \mathcal{L}}{\partial \mathbf{v}} \right) + \boldsymbol{\omega} \times \frac{\partial \mathcal{L}}{\partial \mathbf{v}} &= \left( \frac{\partial \mathbf{f}}{\partial \mathbf{v}} \right)^\top \boldsymbol{\lambda}, \\ \frac{d}{dt} \left( \frac{\partial \mathcal{L}}{\partial \boldsymbol{\omega}} \right) + \boldsymbol{\omega} \times \frac{\partial \mathcal{L}}{\partial \boldsymbol{\omega}} + \mathbf{v} \times \frac{\partial \mathcal{L}}{\partial \mathbf{v}} + \boldsymbol{\gamma} \times \frac{\partial \mathcal{L}}{\partial \boldsymbol{\gamma}} &= \left( \frac{\partial \mathbf{f}}{\partial \boldsymbol{\omega}} \right)^\top \boldsymbol{\lambda} + \left( \frac{\partial g}{\partial \boldsymbol{\omega}} \right) \boldsymbol{\mu}, \end{aligned} \quad (5)$$

where  $\mathcal{L} = T - U$  is the Lagrangian function of the system, and  $\boldsymbol{\lambda}$ ,  $\mu$  are the undetermined multipliers corresponding to the reactions of the constraints (3) and (4), respectively. The undetermined multipliers can be found from the common solution of equations (5) and the time derivatives of the constraints (3) and (4):

$$\boldsymbol{\lambda} = -m((\boldsymbol{\omega} \times \mathbf{r})' + \boldsymbol{\omega} \times (\boldsymbol{\omega} \times \mathbf{r})),$$

$$\mu = \frac{(\boldsymbol{\omega} \times \mathbf{J}\boldsymbol{\omega} + m\mathbf{r} \times (\boldsymbol{\omega} \times \dot{\mathbf{r}}) + mg\boldsymbol{\gamma} \times \mathbf{r}, \mathbf{J}^{-1}\boldsymbol{\gamma})}{(\boldsymbol{\gamma}, \mathbf{J}^{-1}\boldsymbol{\gamma})},$$

where  $\mathbf{J} = \mathbf{I} + m\mathbf{r}^2\mathbf{E}_3 - m\mathbf{r} \otimes \mathbf{r}$  is the tensor of inertia of the body relative to the point of contact. Here  $\mathbf{E}_3$  is the  $3 \times 3$  identity matrix and the symbol  $\otimes$  stands for a tensor multiplication of the vectors which associates to the pair of vectors  $\mathbf{a}$ ,  $\mathbf{b}$  the matrix  $\mathbf{A}$  with components  $A_{i,j} = a_i b_j$ .

After finding the undetermined multipliers and eliminating the velocity  $\mathbf{v}$  (using the constraint (3)), the equations of motion (5) reduce to one vector equation

$$\mathbf{J}\dot{\boldsymbol{\omega}} + \boldsymbol{\omega} \times \mathbf{J}\boldsymbol{\omega} + m\mathbf{r} \times (\boldsymbol{\omega} \times \dot{\mathbf{r}}) + mg\boldsymbol{\gamma} \times \mathbf{r} - \mu\boldsymbol{\gamma} = 0. \quad (6)$$

Adding the kinematic equation of evolution of the vector  $\boldsymbol{\gamma}$  to equation (6), we obtain the following closed reduced system of equations:

$$\begin{aligned} \mathbf{J}\dot{\boldsymbol{\omega}} + \boldsymbol{\omega} \times \mathbf{J}\boldsymbol{\omega} + m\mathbf{r} \times (\boldsymbol{\omega} \times \dot{\mathbf{r}}) + mg\boldsymbol{\gamma} \times \mathbf{r} - \mu\boldsymbol{\gamma} &= 0, \\ \dot{\boldsymbol{\gamma}} &= \boldsymbol{\gamma} \times \boldsymbol{\omega}. \end{aligned} \quad (7)$$

By ‘‘construction’’, this system admits a first integral of motion defined by the constraint (4)  $(\boldsymbol{\omega}, \boldsymbol{\gamma}) = \text{const}$ . The flow defined by equations (7) and restricted to the zero level set of this integral describes the evolution of the variables  $\boldsymbol{\omega}$  and  $\boldsymbol{\gamma}$  in the problem of a body of revolution rolling without slipping or spinning on a horizontal plane.

To reconstruct the velocity of the center of mass, use should be made of the constraint equation (3). The coordinate  $z_c$  is defined from equation (2), and the remaining variables, from the quadratures (1).

### 2.3 Invariants and symmetries

The equations of motion (7) admit the following integrals of motion:

- the energy integral

$$\mathcal{E} = \frac{1}{2}(\mathbf{J}\boldsymbol{\omega}, \boldsymbol{\omega}) - mg(\mathbf{r}, \boldsymbol{\gamma});$$

- the geometric integral

$$\mathcal{F}_0 = (\boldsymbol{\gamma}, \boldsymbol{\gamma}) = 1;$$

- the no-spin constraint (4)

$$\mathcal{F}_1 = (\boldsymbol{\omega}, \boldsymbol{\gamma}) = 0;$$

- the additional integral linear in the angular velocity

$$\mathcal{F}_2 = J(\gamma_3)\omega_3, \quad J(\gamma_3) = \sqrt{i_1\gamma_3^2 + i_3(1 - \gamma_3^2) + m(\mathbf{r}, \boldsymbol{\gamma})^2}.$$

*Remark.* The system (7) admits the energy integral  $\mathcal{E}$  and the additional integral  $\mathcal{F}_2$  only on the zero level set of the integral  $\mathcal{F}_1$ .

*Remark.* We note that in the presence of the constraint (4) the additional integral is expressed in terms of elementary functions for an arbitrary body of revolution, whereas in the classical nonholonomic case the additional integral is written in elementary functions only for the spherical surface of the body.

In addition, equations (7) also admit the invariant measure  $\rho d\boldsymbol{\omega} d\boldsymbol{\gamma}$  with density [14]

$$\rho(\gamma_3) = (i_1 + m\mathbf{r}^2)J(\gamma_3)$$

and possess the symmetry field

$$\boldsymbol{\varsigma} = \omega_1 \frac{\partial}{\partial \omega_2} - \omega_2 \frac{\partial}{\partial \omega_1} + \gamma_1 \frac{\partial}{\partial \gamma_2} - \gamma_2 \frac{\partial}{\partial \gamma_1}, \quad (8)$$

which corresponds to invariance of the system under rotations about the axis of dynamical symmetry of the body.

*Thus, the problem of a body of revolution rolling on a plane without slipping or spinning about the vertical is integrable by the Euler–Jacobi theorem and reduces to quadratures [4].*

## 2.4 Reduction to a system with one degree of freedom

The existence of four integrals of motion allows us to reduce the system (7) to a system with one degree of freedom.

To perform a reduction, we parameterize the vector  $\boldsymbol{\gamma}$  by the nutation angle  $\vartheta$  and the angle of proper rotation  $\varphi$  in the form

$$\gamma_1 = \sin \vartheta \sin \varphi, \quad \gamma_2 = \sin \vartheta \cos \varphi, \quad \gamma_3 = \cos \vartheta. \quad (9)$$

It is easy to show that on the fixed level set of the first integrals

$$\mathcal{F}_0 = 1, \quad \mathcal{F}_1 = 0, \quad \mathcal{F}_2 = k$$

the system of equations (7) reduces to a system with one degree of freedom

$$\begin{aligned} \dot{\vartheta} &= p_{\vartheta}, & \dot{p}_{\vartheta} &= \frac{G(\vartheta)}{B(\vartheta)}, \\ G(\vartheta) &= \left( \frac{k^2 \cot \vartheta}{\sin^2 \vartheta} - \frac{B'(\vartheta)}{2} p_{\vartheta}^2 - \frac{\partial U(\vartheta)}{\partial \vartheta} \right), \end{aligned} \tag{10}$$

where  $B(\vartheta) = i_1 + m r^2$ ,  $U(\vartheta)$  is the potential energy of the system. The system (10) admits the energy integral

$$\mathcal{E} = \frac{B(\vartheta) p_{\vartheta}^2}{2} + \frac{k^2}{2 \sin^2 \vartheta} + U(\vartheta).$$

In this case, the quadrature for angle  $\varphi$  has the form

$$\dot{\varphi} = \frac{\omega_3}{\sin^2 \vartheta},$$

where

$$\omega_3 = \frac{k}{J(\gamma_3)} = \frac{k}{J(\vartheta)}.$$

The values of the variables  $\omega_1$  and  $\omega_2$  can be reconstructed from the relations

$$\begin{aligned} \omega_1 &= \dot{\vartheta} \cos \varphi - \omega_3 \cot \vartheta \sin \varphi, \\ \omega_2 &= -\dot{\vartheta} \sin \varphi - \omega_3 \cot \vartheta \cos \varphi. \end{aligned} \tag{11}$$

Next, we consider the case of an ellipsoid of revolution and perform a complete classification of possible motions of this system.

### 3 Explicit form of the equations of motion for an ellipsoid of revolution

We now turn our attention to a specific body of revolution, an ellipsoid of revolution with semiaxes  $b_1$  and  $b_3$  and with a center of mass displaced along the symmetry axis by distance  $a$  (see Fig. 2).

The radius vector of the point of contact of the ellipsoid can be represented as

$$\mathbf{r} = -\frac{\mathbf{B}\boldsymbol{\gamma}}{\sqrt{(\boldsymbol{\gamma}, \mathbf{B}\boldsymbol{\gamma})}} - a\mathbf{e}_3, \quad \mathbf{B} = \text{diag}(b_1^2, b_1^2, b_3^2).$$

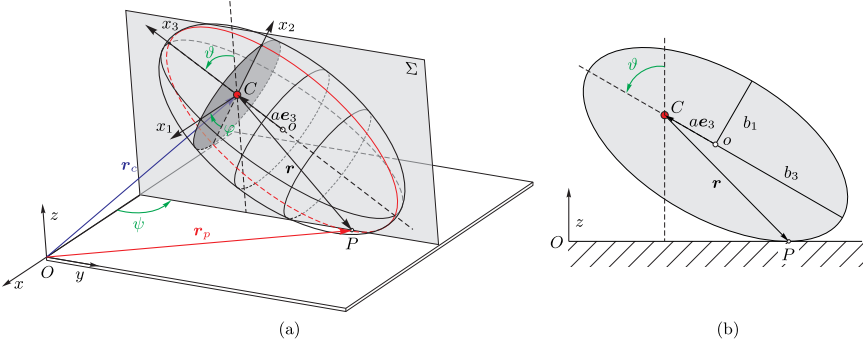


Figure 2: (a) Diagrammatic representation of an ellipsoid on a plane. The plane  $\Sigma$  is a vertical plane passing through the symmetry axis of the ellipsoid. The red elliptic curve is the intersection of the ellipsoid and the plane  $\Sigma$ . (b) Representation of the ellipsoid on the plane in a meridional section.

*Remark.* In this case, the explicit expressions for the functions  $\chi_1(\gamma_3)$  and  $\chi_2(\gamma_3)$  for the case of an ellipsoid of revolution have the form

$$\chi_1(\gamma_3) = -\frac{b_1^2}{\sqrt{b_1^2(1-\gamma_3^2) + b_3^2\gamma_3^2}},$$

$$\chi_2(\gamma_3) = -\frac{b_3^2\gamma_3}{\sqrt{b_1^2(1-\gamma_3^2) + b_3^2\gamma_3^2}} - a.$$

The equations of motion (7) written in the new variables depend on many parameters. In order to decrease their number, we introduce dimensionless parameters: by choosing the length of semiaxis  $b_3$  as a unit of length, the mass of the ellipsoid  $m$  as a unit of mass, and the quantity  $\sqrt{b_3/g}$  as a unit of time, we obtain four dimensionless parameters

$$\alpha = \frac{a}{b_3} \in [0, 1], \quad \beta = \frac{b_1}{b_3} \in (0, \infty),$$

$$\nu = \frac{i_3}{i_1} \in (0, 2], \quad \eta = \frac{mb_3^2}{i_1} \in (0, \infty)$$

and two dimensionless constants of the integrals

$$\varepsilon = \frac{\mathcal{E}}{mgb_3}, \quad \kappa^2 = \frac{k^2}{mgb_3}.$$

The values  $\beta \in (0, 1)$  correspond to an “prolate” ellipsoid, and  $\beta \in (1, \infty)$ , to an “oblate” one. In the limiting case  $\beta = 0$  we obtain a thin rod, and for  $\beta \rightarrow \infty$  we obtain a thin disk. However, these cases correspond to the motion of a body with a sharp edge, which we do not consider in this paper.

After transformation to the new variables and nondimensionalization for the case of an ellipsoid of revolution, the potential energy  $U(\vartheta)$  takes the form

$$U(\vartheta) = \alpha \cos \vartheta + Z(\vartheta),$$

$$Z(\vartheta) = \sqrt{\beta^2 \sin^2 \vartheta + \cos^2 \vartheta} > 0 \quad \forall \vartheta \in [0, \pi],$$

and the equations of motion (10) can be written as

$$\dot{\vartheta} = p_\vartheta,$$

$$\dot{p}_\vartheta = \frac{1}{B(\vartheta)} \left( \frac{\kappa^2 \cot \vartheta}{\sin^2 \vartheta} - \frac{B'(\vartheta)}{2} p_\vartheta^2 + \alpha \sin \vartheta + \frac{(1 - \beta^2) \sin \vartheta \cos \vartheta}{Z(\vartheta)} \right),$$

where

$$B(\vartheta) = \frac{1}{\eta} + \frac{1}{Z(\vartheta)^2} (\beta^4 \sin^2 \vartheta + (\alpha Z(\vartheta) - \cos \vartheta)^2).$$

We note here that the physical meaning of  $Z(\vartheta)$  is the height of the geometric center of the ellipsoid above the supporting plane.

Next, we perform a complete classification of possible motions of the resulting system.

## 4 Bifurcation analysis

### 4.1 General definitions

To classify the motions of the system, we use the topological approach described in [50, 51]. For this we consider the system (7) in the redundant coordinates  $\mathbf{z} = (\boldsymbol{\omega}, \boldsymbol{\gamma})$ , which defines the phase flow in the space  $\mathcal{M}_6 = \{\mathbf{z}\}$ . This system possesses four integrals of motion  $\mathcal{F}_0$ ,  $\mathcal{F}_1$ ,  $\mathcal{F}_2$ , and  $\mathcal{E}$ . We restrict the system (7) to the common level set of the integrals  $\mathcal{F}_0$  and  $\mathcal{F}_1$

$$\mathcal{M}_4 = \{\mathbf{z} \mid \mathcal{F}_0 = 1, \mathcal{F}_1 = 0\} \subset \mathcal{M}_6.$$

Let us define the integral map of this system  $\Phi : \mathcal{M}_4 \rightarrow \mathbb{R}^2$

$$\mathbf{z} \rightarrow \Phi(\mathbf{z}) = (\mathcal{F}_2(\mathbf{z}), \mathcal{E}(\mathbf{z})) \in \mathbb{R}^2, \quad \mathbf{z} \in \mathcal{M}_4.$$

*Remark.* As local coordinates on  $\mathcal{M}_4$  we can choose, for example, the quantities  $(\vartheta, \varphi, \omega_1, \omega_2)$ . However, some solutions of interest lie on the singularities of the chosen coordinates  $(\vartheta = 0, \pi)$ . Therefore, it is more convenient to perform calculations in the redundant coordinates.

The complete image of the phase space  $\Phi(\mathcal{M}_4)$  defines the *region of possible motions (RPM)* of the system on the plane of first integrals  $(\kappa, \varepsilon)$ . Each point on the plane of first integrals  $(\kappa, \varepsilon)$  corresponds to the integral manifold

$$\mathcal{M}_{\kappa, \varepsilon} = \{z \mid \mathcal{F}_0 = 1, \mathcal{F}_1 = 0, \mathcal{F}_2(z) = \kappa, \mathcal{E}(z) = \varepsilon\} \subset \mathcal{M}_6,$$

which can contain several connectedness components (generally two-dimensional tori).

Changes in the values of the integrals  $\kappa$  and  $\varepsilon$  lead to bifurcations of the integral manifolds. These bifurcations correspond to a *critical set* of the integral map which is defined as follows:

$$S = \{z \in \mathcal{M}_4 \mid \text{rank } d\Phi < 2\}.$$

The image of the critical set  $S$  in the space of first integrals  $\Phi(S)$  and the region of possible motions  $\Phi(\mathcal{M}_4)$  form a *bifurcation diagram* of the integrable system.

The set  $S$  is a union of two subsets:

$$\begin{aligned} S_0 &= \{z \in \mathcal{M}_4 \mid \text{rank } d\Phi = 0\}, \\ S_1 &= \{z \in \mathcal{M}_4 \mid \text{rank } d\Phi = 1\}. \end{aligned}$$

In the case at hand the subset  $S_0$  consists of separate points, and the subset  $S_1$  is a one-parameter family of closed curves. The points belonging to  $S_0$  are the fixed points of the system (7), and the set  $S_1$  is filled by periodic solutions of the system (7), which correspond to fixed points of the reduced system (10).

## 4.2 Critical sets

To find the sets  $S_1$  or  $S_0$  in redundant coordinates, it is necessary to solve the system of equations given by the equations

$$\text{rank} \left. \frac{\partial(\mathcal{F}_0, \mathcal{F}_1, \mathcal{F}_2, \mathcal{E})}{\partial z} \right|_{\mathcal{M}_4} = 3 \quad (12)$$

or

$$\text{rank} \left. \frac{\partial(\mathcal{F}_0, \mathcal{F}_1, \mathcal{F}_2, \mathcal{E})}{\partial z} \right|_{\mathcal{M}_4} = 2, \quad (13)$$

respectively. This can be done, for example, using the method of undetermined multipliers (see, e.g., [52]). We will not present here this procedure in explicit form since it is standard and the intermediate expressions are cumbersome.

Next, we consider each of the critical subsets separately.

#### 4.2.1 The critical subset $S_1$

Analysis of equations (12) shows that they can have different solutions, depending on whether or not the parameter  $\alpha$  is equal to zero. We first consider the general case  $\alpha \neq 0$ .

Solving the system of equations given by (12), we can prove the following proposition.

**Proposition.** *In the case  $\alpha \neq 0$  the critical subset  $S_1$  of the integral map  $\Phi$  has the form*

$$S_1 = S_1^\alpha = \{z \mid \omega = \omega_0(\vartheta)\gamma \times (\mathbf{e}_3 \times \gamma), \gamma = \gamma(\vartheta, \varphi)\},$$

where the dependence  $\gamma(\vartheta, \varphi)$  is defined by the expressions (9),  $\omega_0(\vartheta)$  has the form

$$\omega_0^2 = \frac{-\eta \sin^2 \vartheta (\cos \vartheta (1 - \beta^2) + \alpha Z(\vartheta))}{\cos \vartheta Z(\vartheta) (\eta (Z(\vartheta) + \alpha \cos \vartheta)^2 + \cos^2 \vartheta + \nu \sin^2 \vartheta)}, \quad (14)$$

$\varphi \in [0, 2\pi)$ , and the range of angle  $\vartheta$  is determined from the condition that the expression (14) be nonnegative for  $\omega_0^2$ .

The critical set  $S_1^\alpha$  is filled by periodic trajectories for which the dependences  $\vartheta(t)$  and  $\varphi(t)$  have the form

$$\vartheta = \vartheta_0 = \text{const}, \quad \varphi = \varphi_0 + \frac{\omega_0}{\sin \vartheta_0} t, \quad (15)$$

where  $\varphi_0 \in [0, 2\pi)$  defines the initial angle of proper rotation. Due to the axial symmetry of the system, without loss of generality, one can set  $\varphi_0 = 0$ . As is customary, we will call the solutions (15) *permanent rotations*. In the reduced system (10) they correspond to a one-parameter family of fixed points

$$\vartheta = \vartheta_0 = \text{const}, \quad p_\vartheta = 0. \quad (16)$$

In the problem we consider here, under permanent rotations, the trajectory of the ellipsoid in the fixed coordinate system is closed and the following proposition holds.

**Proposition.** *The fixed points (16) correspond to the rolling of an ellipsoid in a circle with a constant inclination angle of the symmetry axis,  $\vartheta_0$ . The point of contact traces out a circle of radius  $\rho_p = \frac{\beta^2}{Z(\vartheta_0)} \tan \vartheta_0$ , and the center of mass traces out a circle of radius  $\rho_c = Z(\vartheta_0) \tan \vartheta_0 + \alpha \sin \vartheta_0$ .*

*Proof.* Let us parameterize the rotation matrix  $\mathbf{Q}$  by Euler's angles: the nutation angle  $\vartheta$ , the precession angle  $\psi$  and the angle of proper rotation  $\varphi$  (we have already introduced two of the three angles above for parameterization of the vector  $\boldsymbol{\gamma}$ ) [49]

$$\mathbf{Q} = \begin{pmatrix} \cos \psi \cos \varphi - \cos \vartheta \sin \psi \sin \varphi & \sin \psi \cos \varphi + \cos \vartheta \cos \psi \sin \varphi & \sin \varphi \sin \vartheta \\ -\cos \psi \sin \varphi - \cos \vartheta \sin \psi \cos \varphi & -\sin \psi \sin \varphi + \cos \vartheta \cos \psi \cos \varphi & \cos \varphi \sin \vartheta \\ \sin \vartheta \sin \psi & -\sin \vartheta \cos \psi & \cos \vartheta \end{pmatrix}.$$

The quadrature for angle  $\psi$ , with (1) and (11) taken into account, has the form

$$\dot{\psi} = -\frac{\kappa \cos \vartheta}{J(\vartheta) \sin^2 \vartheta}. \quad (17)$$

Thus, for the solution (15) the dependence  $\psi(t)$  has the form

$$\psi = \psi_0 + \omega_\psi t, \quad \omega_\psi = -\frac{\kappa \cos \vartheta_0}{J(\vartheta_0) \sin^2 \vartheta_0} = \text{const},$$

where  $\psi_0$  is the initial value of angle  $\psi$ , which without loss of generality can be set equal to zero  $\psi_0 = 0$ .

In accordance with (15), angle  $\varphi$  also changes linearly in time

$$\varphi = \varphi_0 + \omega_\varphi t, \quad \omega_\varphi = \frac{\kappa}{J(\vartheta_0) \sin^2 \vartheta_0} = \text{const},$$

where the initial value of angle  $\varphi_0$  will also be assumed to be zero.

Substituting the resulting expressions into the quadratures (1) and integrating them over time, we obtain

$$x_c = \rho_c \sin \psi, \quad y_c = -\rho_c \cos \psi, \quad z_c = \alpha \cos \vartheta_0 + Z(\vartheta_0),$$

where  $\rho_c = Z(\vartheta_0) \tan \vartheta_0 + \alpha \sin \vartheta_0$ .

Knowing the trajectory of the center of mass  $\mathbf{r}_c(t)$ , we find the trajectory of the point of contact from the relation

$$\mathbf{r}_p = \mathbf{r}_c + \mathbf{Q}\mathbf{r},$$

where  $\mathbf{r}_p = (x_p, y_p, 0)$  is the radius vector of the point of contact referred to the fixed coordinate system. This yields

$$x_p = x_c + (\mathbf{r}, \boldsymbol{\alpha}) = \rho_p \sin \psi, \quad y_p = y_c + (\mathbf{r}, \boldsymbol{\beta}) = -\rho_p \cos \psi,$$

where  $\rho_p = \frac{\beta^2}{Z(\vartheta_0)} \tan \vartheta_0$ .

□

From the resulting expressions for the radius of the circle of the trajectory of the contact point and the center of mass it can be seen that, as  $\vartheta_0 \rightarrow \pi/2$ ,  $\rho_c \rightarrow \infty$  and  $\rho_p \rightarrow \infty$ . That is, as the symmetry axis approaches the horizontal position, the radius of the circle increases without bound. Figure 3 shows a schematic representation of permanent rotations of an ellipsoid of revolution on a plane.

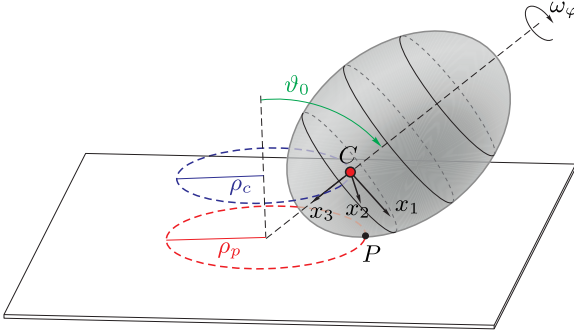


Figure 3: Example of permanent rotations of an ellipsoid

Note that, for fixed values of the parameters  $\alpha$  and  $\beta$ , permanent rotations are not possible for all inclination angles of the symmetry axis of the ellipsoid  $\vartheta_0$ . Possible inclination angles are defined by the inequality  $\omega_0^2(\vartheta) \geq 0$ . Figure 4 shows the regions on the plane  $(\beta^2, \vartheta)$  that are given by this inequality for a fixed value of  $\alpha$ .

*Remark.* In [53] conditions are found for the parameters of an ellipsoid under which permanent rotations may occur at any point of the ellipsoid's surface, and in [54] the stability of such rotations is analyzed.

Analyzing the expression (14) and Fig. 4, we can formulate the following statements.

**Statement 1.** *Permanent rotations under which the center of mass of the ellipsoid lies above its geometric center exist only for a fairly oblate ellipsoid ( $\beta^2 > 1 + \alpha$ ).*

**Statement 2.** *Permanent rotations under which the center of mass of the ellipsoid lies below its geometric center exist regardless of the form of the*

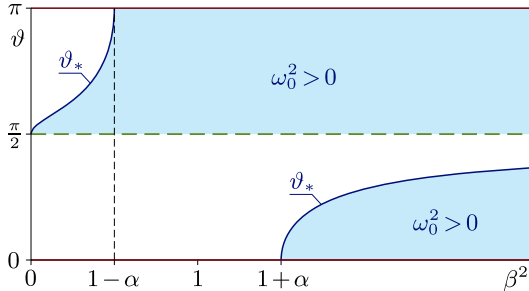


Figure 4: Regions of positive definiteness of the expression (14) on the parameter plane  $(\beta^2, \vartheta)$  for a fixed value of  $\alpha$ .

*ellipsoid. However, for a fairly prolate ellipsoid ( $\beta^2 < 1 - \alpha$ ) such rotations are possible only for a fairly large inclination angle of its symmetry axis.*

In addition, it follows from the analysis of the expression (14) and Fig. 4 that there exist inclined equilibrium positions of the ellipsoid. These equilibrium positions are defined from the condition  $\omega_0^2 = 0$ . The inclination angle for such equilibrium positions depends on the parameters of the ellipsoid as follows:

$$\vartheta_* = \arccos \frac{\alpha\beta}{\sqrt{(1-\beta^2)(1+\alpha^2-\beta^2)}}. \quad (18)$$

In Fig. 4, these equilibrium positions correspond to the boundary of the region  $\omega_0^2 \geq 0$ . These positions exist only under some restrictions on the mass-geometric parameters of the ellipsoid. These restrictions have a simple mechanical interpretation.

**Statement 3.** *The inclined equilibrium positions of an ellipsoid of revolution with axisymmetric mass distribution exist only when its center of mass lies between the centers of curvature of its vertices.*

In the case  $\alpha = 0$  (without displacement of the center of mass), additional symmetry leads to an increase in the critical set  $S_1$ .

**Proposition.** *In the case  $\alpha = 0$  the critical subset  $S_1$  of the integral map*

$\Phi$  is a union of two subsets

$$S_1 = S_1^\alpha \cup S_1^0,$$

$$S_1^0 = \{(\boldsymbol{\omega}, \boldsymbol{\gamma}(\vartheta, \varphi)) \mid \boldsymbol{\omega} = (0, 0, \omega_3), \vartheta = \frac{\pi}{2},$$

$$\varphi \in [0, 2\pi), \omega_3 \in \mathbb{R}\}.$$

The critical subset  $S_1^0$  is filled by periodic trajectories

$$\omega_3 = \omega_0 = \text{const}, \quad \vartheta = \frac{\pi}{2}, \quad \varphi = \varphi_0 + \omega_0 t. \quad (19)$$

In the reduced system (10) all solutions (19) correspond to one fixed point

$$\vartheta = \frac{\pi}{2}, \quad p_\vartheta = 0.$$

In the fixed coordinate system, the solutions (19) correspond to the rolling along the ellipsoid's equator in a straight line with an arbitrary velocity.

#### 4.2.2 The critical subset $S_0$

We now consider the critical subset  $S_0$ . Solving the system of equations given by equation (13), we can prove the following proposition.

**Proposition.** *The critical subset  $S_0$  of the integral map  $\Phi$  consists of two points*

$$S_0 = S_0^\pm = \{(\boldsymbol{\omega}, \boldsymbol{\gamma}) \mid \boldsymbol{\omega} = 0, \boldsymbol{\gamma} = (0, 0, \pm 1)\}.$$

The critical subset  $S_0$  is filled by fixed points of the system (7). These points correspond to the equilibrium positions of the ellipsoid in which it rests on one of its vertices. In Fig. 4, the fixed points  $S_0$  correspond to the horizontal straight lines  $\vartheta = 0$  and  $\vartheta = \pi$ .

*Remark.* The fixed points of the complete system (7)  $S_0$  correspond to fixed points of the reduced system (10). This is due to the fact that such equilibrium positions lie on singular zero-dimensional orbits of the action of the rotation group (8).

### 4.3 Example of a bifurcation diagram

Consider an example of constructing a bifurcation diagram which is an image of the critical set  $S$ . We present the explicit form of bifurcation curves and points corresponding to the image  $\Phi(S)$ :

- the image of the subset  $S_1^\alpha$  consists of curves on the plane of first integrals  $(\kappa, \varepsilon)$ , which can be represented as

$$\sigma_\vartheta : \begin{cases} \varepsilon = \frac{3Z(\vartheta_0)^2 - 1}{2Z(\vartheta_0)} + \alpha \frac{3 \cos^2 \vartheta_0 - 1}{2 \cos \vartheta_0}, \\ \kappa = \pm \sin^2 \vartheta_0 \sqrt{\frac{\beta^2 - 1}{Z(\vartheta_0)} - \frac{\alpha}{\cos \vartheta_0}}, \end{cases} \quad (20)$$

where

$$\begin{aligned} \vartheta_0 &\in (\pi/2, \vartheta_*) \quad \text{for } \beta^2 < 1 - \alpha, \\ \vartheta_0 &\in (\pi/2, \pi) \quad \text{for } 1 - \alpha < \beta^2 < 1 + \alpha, \\ \vartheta_0 &\in (0, \vartheta_*] \cup (\pi/2, \pi) \quad \text{for } \beta^2 > 1 + \alpha; \end{aligned}$$

- the image of the subset  $S_1^0$  is a parabola

$$\sigma_{\pi/2} : \varepsilon = \frac{\kappa^2}{2} + \beta; \quad (21)$$

- the image of the subset  $S_0$  on the plane of first integrals  $(\kappa, \varepsilon)$  consists of a pair of point

$$\sigma_0 : (0, 1 + \alpha), \quad \sigma_\pi : (0, 1 - \alpha). \quad (22)$$

Depending on the values of the parameters  $\alpha$  and  $\beta$ , these points can be isolated. It can be seen from Fig. 4 that the point  $\sigma_0$  is isolated when  $\beta^2 < 1 + \alpha$ , and the point  $\sigma_\pi$ , when  $\beta^2 < 1 - \alpha$ . We note that in the case  $\alpha = 0$  these points lie on the same level set of the integral  $\kappa = 0, \varepsilon = 1$ , but do not coincide in  $\mathcal{M}_6$ .

Figure 5 shows an example of constructing a bifurcation diagram on the plane of first integrals  $(\kappa, \varepsilon)$  for the general case  $\alpha \neq 0$ . This example of a bifurcation diagram is given for the case of an “oblate” ellipsoid  $\beta^2 > 1$  with a relatively small displacement of the center of mass. In this section, we explain the notation used in the diagram, and in the following sections we will use them without repeating our explanations.

In the diagram, gray denotes the region of possible motions of the system. In the light gray region, the integral manifold is two-dimensional torus  $\mathbb{T}^2$ . Dark gray denotes the region which corresponds to two connectedness components of the integral manifold (two two-dimensional tori  $2\mathbb{T}^2$ ). These two connectedness components are glued together to each other along the curve  $\sigma_u$ . In the white region, no motions of the system are possible ( $\emptyset$ ).

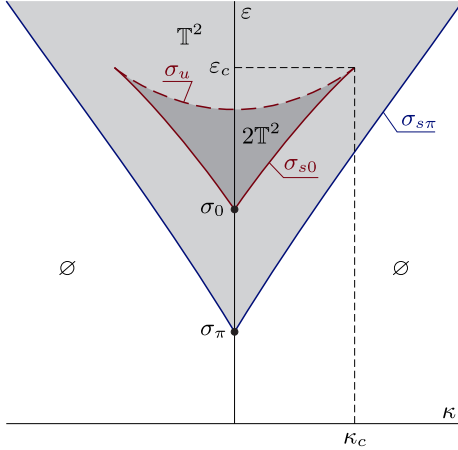


Figure 5: Example of a bifurcation diagram. This type of diagram is characteristic of an “oblate” ellipsoid with a fairly small displacement of the center of mass  $\alpha$ .

The heavy solid and dotted lines in the diagram show parts of the bifurcation curves (20) (and (21) for the case  $\alpha = 0$ ). The solid curves correspond to stable fixed points, and the dotted curves indicate unstable ones. The curve (20) is partitioned by critical values of angle  $\vartheta_0$  into separate segments with the same type of stability, which are denoted in the diagram by different symbols. The curve  $\sigma_{s\pi}$  corresponds to  $\vartheta_0 \in (\pi/2, \pi)$ , the curve  $\sigma_{s0}$  corresponds to  $\vartheta_0 \in (0, \vartheta_c)$ , and the curve  $\sigma_u$ , to  $\vartheta_0 \in (\vartheta_c, \vartheta_*]$ . Here  $\vartheta_c$  is the critical value of angle  $\vartheta_0$ . At this value,  $\vartheta_0 = \vartheta_c$  (which corresponds to the point  $(\kappa_c, \varepsilon_c)$  in the diagram), one can observe a change in the type of stability of fixed points corresponding to the curve  $\sigma_\vartheta$ . The fixed points (22) corresponding to equilibrium positions are shown as colored black points (in the case of their stability) or punctured points (in the case of their instability).

As the parameters of the system  $\alpha, \beta$  change, the critical subsets  $S_1$  and  $S_0$  can change, resulting in a qualitative change in the type of the diagram. The bifurcations of critical points described above occur simultaneously with this change. In order to determine possible types of bifurcation diagrams, we investigate the bifurcations of critical points in what follows.

## 4.4 Bifurcations of critical sets and types of bifurcation diagrams

### 4.4.1 Bifurcations of the critical subset $S_0$

Consider the bifurcations of the critical subset  $S_0$ .

When  $\beta^2 < 1 - \alpha$  (see Fig. 4), the subset  $S_0$  consists of two isolated points. When  $\beta^2 = 1 - \alpha$ , a bifurcation occurs, resulting in the component  $S_0^-$  merging with the component  $S_1^\alpha$ .

Next, when  $1 - \alpha < \beta^2 < 1 + \alpha$ , one of the points of the subset  $S_0$  is isolated ( $S_0^+$ ) and the other is not isolated ( $S_0^-$ ).

When  $\beta^2 = 1 + \alpha$ , a second bifurcation occurs during which the component  $S_1^\alpha$  is born from  $S_0^+$ , and both points of the subset  $S_0$  are not isolated now.

We note that, simultaneously with the bifurcations of critical sets described above, changes in the stability of the fixed points occur. To illustrate this fact, we analyze the linear stability of the fixed points

$$\vartheta = 0, \quad p_\vartheta = 0 \quad \text{and} \quad \vartheta = \pi, \quad p_\vartheta = 0 \quad (23)$$

of the reduced system (10).

To do so, we represent the system (10) as

$$\dot{\mathbf{q}} = \mathbf{f}(\mathbf{q}),$$

where  $\mathbf{q} = (\vartheta, p_\vartheta)$ ,  $\mathbf{f}(\mathbf{q})$  is the vector function whose elements depend on the components of  $\mathbf{q}$ . Introducing the perturbation vector  $\tilde{\mathbf{q}} = \mathbf{q} - \mathbf{q}_0$ , where  $\mathbf{q}_0 = (\vartheta_0, 0)$  is the equilibrium position, and representing the equation for  $\tilde{\mathbf{q}}$  as a series expansion near the equilibrium position, we obtain

$$\dot{\tilde{\mathbf{q}}} = \mathbf{\Lambda} \tilde{\mathbf{q}}, \quad \mathbf{\Lambda} = \left. \frac{\partial \mathbf{f}(\mathbf{q})}{\partial \mathbf{q}} \right|_{\mathbf{q}=\mathbf{q}_0}.$$

The matrix  $\mathbf{\Lambda}$  has the form

$$\mathbf{\Lambda} = \begin{pmatrix} 0 & 1 \\ \frac{G'_0(\vartheta_0)}{B(\vartheta_0)} & 0 \end{pmatrix},$$

where the notation  $G_0(\vartheta_0) = G(\vartheta_0)|_{p_\vartheta=0}$  is used, i.e.,  $G'_0(\vartheta_0)$  denotes the derivative of the function  $G(\vartheta)$  with respect to  $\vartheta$ , calculated at the point  $\vartheta_0$  for  $p_\vartheta = 0$ .

We write the characteristic equation

$$\det(\mathbf{\Lambda} - \lambda \mathbf{E}_2) = 0,$$

where  $\lambda$  are the eigenvalues of the matrix  $\mathbf{\Lambda}$  and  $\mathbf{E}_2$  is the  $2 \times 2$  identity matrix. This equation reduces to the simple quadratic equation

$$\lambda^2 - \frac{G'_0(\vartheta_0)}{B(\vartheta_0)} = 0.$$

Since  $B(\vartheta_0) > 0$  for any values of  $\vartheta_0$ , the eigenvalues of  $\lambda$  are defined by the value of  $G'_0(\vartheta_0)$ . If  $G'_0(\vartheta_0) < 0$ , the corresponding fixed point is a stable center-type point. If  $G'_0(\vartheta_0) > 0$ , then the corresponding fixed point is an unstable saddle point.

For the lower equilibrium position ( $\vartheta_0 = \pi$ ,  $\kappa = 0$ ) the value of  $G'_0(\vartheta_0)$  is negative for  $\beta^2 > 1 - \alpha$ , and for the upper equilibrium position ( $\vartheta_0 = 0$ ,  $\kappa = 0$ ) it is negative for  $\beta^2 > 1 + \alpha$ . Thus, depending on the type of stability of the fixed points (23), the parameter plane  $(\alpha, \beta^2)$  can be divided into three regions:

- (a)  $\beta^2 < 1 - \alpha$ . In this region, both fixed points  $\sigma_0$ ,  $\sigma_\pi$  are unstable and isolated;
- (b)  $1 - \alpha < \beta^2 < 1 + \alpha$ . In this region, the lower position of the ellipsoid  $\sigma_\pi$  is stable and is nonisolated, and the upper one,  $\sigma_0$ , is unstable and isolated;
- (c)  $\beta^2 > 1 + \alpha$ . In this region, both fixed points are stable  $\sigma_0$ ,  $\sigma_\pi$  and nonisolated.

*Remark.* We note that the resulting boundaries of the stability of the solutions  $\sigma_0$  and  $\sigma_\pi$  are defined only by the geometry of the body and the position of the center of mass. For the stability of the vertical position of the ellipsoid it is necessary that its center of mass ( $1 \pm \alpha$ ) be below the center of curvature ( $\beta^2$ ) of the ellipsoid's surface at the point of contact. The center of curvature in this case is correctly determined because the body is axisymmetric and the principal radii of curvature at the vertices of the ellipsoid are the same. This statement is in agreement with the results obtained in the book [55] for an arbitrary body of revolution and in our recent paper [13] on the dynamics of an ellipsoid on a vibrating plane.

#### 4.4.2 Bifurcations of critical subsets $S_1$

We now turn our attention to bifurcations of the critical subset  $S_1$ , which corresponds to the fixed points (16) of the reduced system (10). The topological type of the subset  $S_1$  is uniquely related to the type of the bifurcation

curve (20). The type of bifurcation curve is determined, in its turn, by its critical points, which satisfy the system of equations

$$G_0(\vartheta) = 0, \quad \frac{\partial G_0(\vartheta)}{\partial \vartheta} = 0. \quad (24)$$

In the bifurcation diagram, these critical points correspond to the cusp points and tangency points of the bifurcation curves; also, the bifurcation curves can lose smoothness at these points.

Let us analyze the bifurcations of the critical points depending on the values of the parameters  $\alpha$  and  $\beta$ .

The emergence of new critical points is defined by the additional condition

$$\frac{\partial^2 G_0(\vartheta)}{\partial \vartheta^2} = 0. \quad (25)$$

The common solution of the system of equations (24)–(25) defines the curve on the plane  $(\alpha, \beta^2)$  which separates regions with different numbers of critical points and hence with different types of bifurcation diagrams.

In the case  $\alpha \neq 0$ , the system of equations (24)–(25) gives two solutions:

1.  $\beta^2 = 1 + \alpha$ . This straight line on the plane  $(\alpha, \beta^2)$  separates the regions with one cusp point (with  $\beta^2 > 1 + \alpha$ ) and without cusp points (with  $\beta^2 < 1 + \alpha$ ). In addition, as shown in the preceding section, when this straight line is intersected, a bifurcation curve  $\sigma_\vartheta$  (branches  $\sigma_{s_0}$  and  $\sigma_u$ ) is born from point  $\sigma_0$ , and  $\sigma_0$  ceases to be isolated.
2.  $\beta^2 = 1 - \alpha$ . This straight line on the plane  $(\alpha, \beta^2)$  corresponds to the loss of smoothness of the bifurcation curve  $\sigma_{s\pi}$  with  $\kappa = 0$ , in which case the point  $\sigma_\pi$  descends to the bifurcation curve  $\sigma_{s\pi}$  and ceases to be isolated.

As we see, the bifurcations of  $S_1$  listed above occur at the same time as those of  $S_0$ . This system has no other bifurcations of  $S_1$  which do not affect  $S_0$ .

As was shown above, when  $\alpha = 0$  the subset  $S_1$  bifurcates. Next, we consider the question of bifurcations of  $S_1$  for constant  $\alpha = 0$  and for the varying parameter  $\beta$ . In the case  $\alpha = 0$  the system of equations (24)–(25) has a unique solution  $\beta^2 = 1$ . For  $\beta^2 < 1$  there exists only one curve  $\sigma_{\pi/2}$  on the plane of first integrals, and the fixed points  $\sigma_0$  and  $\sigma_\pi$  are isolated. When  $\beta^2 = 1$ , bifurcation curves  $\sigma_{s_0}$  and  $\sigma_{s\pi}$  are born from the points  $\sigma_0$  and  $\sigma_\pi$ , respectively. The points  $\sigma_0$  and  $\sigma_\pi$  cease to be isolated, and on the

curve  $\sigma_{\pi/2}$  tangency points are born at which the curves  $\sigma_{s_0}$  and  $\sigma_{s_\pi}$  are tangent to the curve  $\sigma_{\pi/2}$ .

Simultaneously, the stability of the fixed point corresponding to the curve  $\sigma_{\pi/2}$  changes. Indeed, following the above-mentioned algorithm of the linear stability analysis of fixed points, the condition for stability is defined by the sign  $G'_0(\pi/2)$ , whence we find that the point (19) is stable for

$$|\kappa| < \kappa_c = \sqrt{\frac{\beta^2 - 1}{\beta}}. \quad (26)$$

From this, we obtain the critical value of the parameter

$$\beta^2 = 1.$$

Thus, when  $\beta^2 < 1$  the fixed point

$$\vartheta = \frac{\pi}{2}, \quad p_\vartheta = 0$$

is stable for any values of  $\kappa$ , and for  $\beta^2 > 1$  it is stable only when condition (26) is satisfied.

#### 4.4.3 Types of bifurcation diagrams

Summarizing, we note that the entire parameter space  $(\alpha, \beta^2)$  can be divided into five regions corresponding to different types of bifurcation diagrams (see Fig. 6). Figure 7 shows all possible types of bifurcation diagrams for the problem under consideration. Diagrams (a)–(c) correspond to the general case  $\alpha > 0$  and have been constructed for the fixed value  $\alpha = 0.5$  and different values of  $\beta$ , and diagrams (c) and (d), for the case  $\alpha = 0$ .

Next, we consider in more detail each of the types of diagrams. In the names of the types of diagrams (a)–(e) we refer to Fig. 7. In addition, for each type of diagrams we construct all possible types of phase portraits of the reduced system (10) on different level sets of the integral  $\mathcal{F}_2$ .

#### 4.4.4 Bifurcation diagram (a)

Figure 8 shows a bifurcation diagram and the corresponding phase portraits for the case where the bifurcation diagram has no cusp points for  $\alpha \neq 0$ . As can be seen from this figure, both points  $s_0$  and  $s_\pi$  do not lie on the bifurcation curve  $\sigma_\vartheta$  and are isolated.

For this case, two types of qualitatively different phase portraits are possible: for  $\kappa = 0$  and for  $|\kappa| > 0$ . In Fig. 8, the points  $s_0$  and  $s_1$  denote

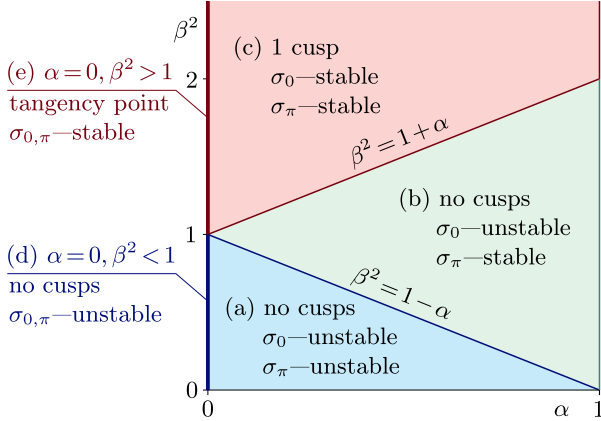


Figure 6: Regions with different types of bifurcation diagrams on the parameter plane  $(\alpha, \beta^2)$ .

fixed points of the family  $\sigma_{\vartheta}$  which lie on the chosen level sets of the first integral  $\kappa = 0$  and  $\kappa = 1$ , respectively.

As can be seen from Fig. 8a, for the case  $\kappa = 0$  the phase trajectories pass through the poles  $\vartheta = 0$  and  $\vartheta = \pi$ . For a correct passage through the pole, it is necessary to glue together the trajectories in the phase portrait:  $\vartheta \rightarrow -\vartheta$ . Thus, in this case each level set of the first integrals corresponds to one connectedness component, which is in complete agreement with the bifurcation diagram.

#### 4.4.5 Bifurcation diagram (b)

As the parameter  $\beta$  increases, the curve  $\sigma_{s\pi}$  approaches the point  $\sigma_{\pi}$ . When  $\beta^2 = 1 - \alpha$ , the point  $\sigma_{\pi}$  descends to the bifurcation curve  $\sigma_{s\pi}$ . Also,  $\sigma_{\pi}$  ceases to be isolated, and the branch  $\sigma_{s\pi}$  loses smoothness at this point ( $\kappa = 0$ ). The corresponding type of diagram and the phase portraits are presented in Fig. 9.

*Remark.* A similar bifurcation, not when the parameter, but the level set of the integrals is changed, can be observed in the classical problem of the Lagrange top. The corresponding conditions for stability of a sleeping top are called the Maievsky condition [49, 55].

For this case also, only two types of qualitatively different phase portraits similar to diagram (a) are possible. The only difference is that the

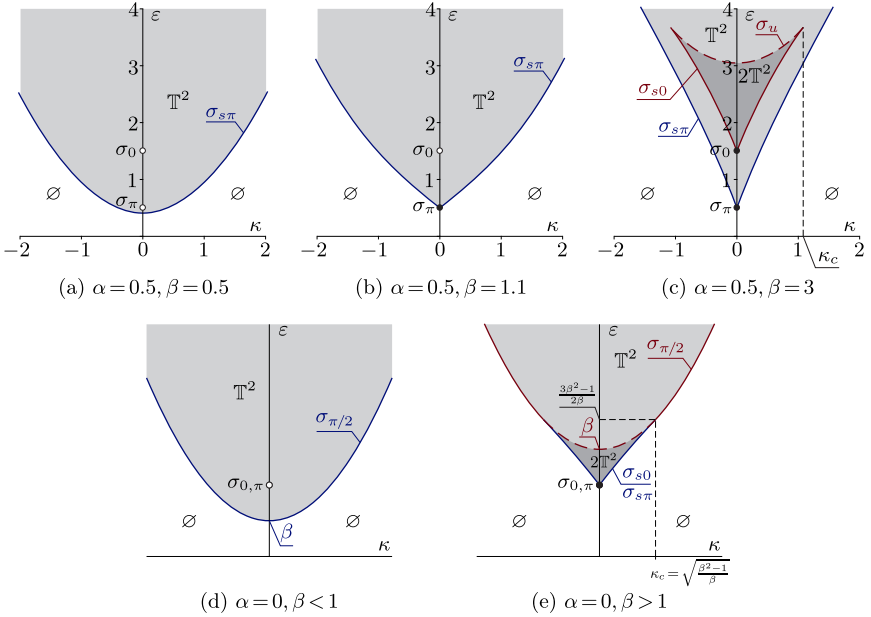


Figure 7: Possible types of bifurcation diagrams for (a)–(c)  $\alpha = 0.5$  and (d), (e)  $\alpha = 0$ .

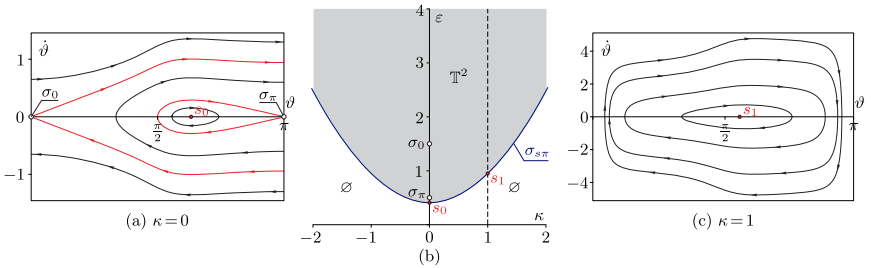


Figure 8: Bifurcation diagram (b) and examples of phase portraits (a), (c) corresponding to different values of the integral  $\kappa$  for  $\alpha = 0.5, \beta = 0.5$ .

point  $\sigma_\pi$  is stable for  $\kappa = 0$ .

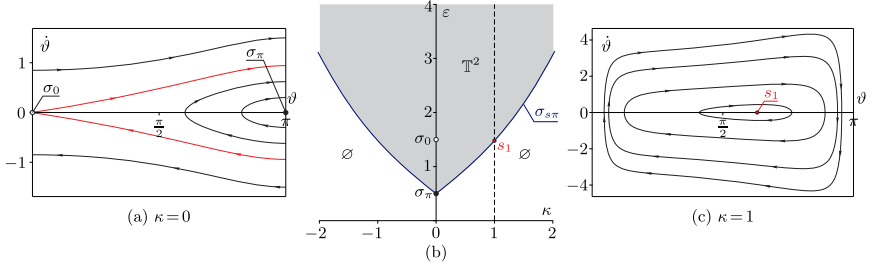


Figure 9: Bifurcation diagram (b) and examples of phase portraits (a), (c) corresponding to different values of the integral  $\kappa$  for  $\alpha = 0.5$ ,  $\beta = 1.1$ .

#### 4.4.6 Bifurcation diagram (c)

Further increase in the parameter  $\beta$ , with  $\beta^2 = 1 + \alpha$ , leads to a new bifurcation. The second isolated point  $\sigma_0$  gives rise to bifurcation branches  $\sigma_{s_0}$  and  $\sigma_u$ . The corresponding diagram and the phase portraits are presented in Fig. 10.

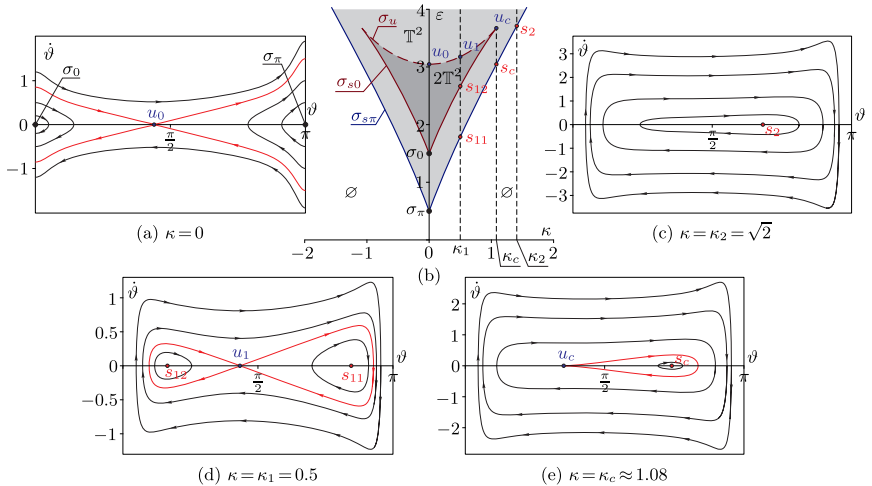


Figure 10: Bifurcation diagram (b) and examples of phase portraits (a), (c)–(e) corresponding to different values of the integral  $\kappa$  for  $\alpha = 0.5$ ,  $\beta = 3$ .

As can be seen from the figure, in this case there exist four different types of phase portraits. When  $\kappa = 0$  and  $0 < |\kappa| < \kappa_c$  (Figs. 10a, 10d) the

phase portrait has three fixed points: two of them are stable ( $\sigma_0$ ,  $\sigma_\pi$  for  $\kappa = 0$  and  $s_{11}$ ,  $s_{12}$  for  $\kappa = \kappa_1$ ) and one is unstable ( $u_0$  and  $u_1$ , respectively). When  $\kappa = \kappa_c$  (Fig. 10e) the curves  $\sigma_u$  and  $\sigma_{s_0}$  merge at the point  $u_c$ . In this case, the phase portrait exhibits a saddle-node bifurcation — the stable point and the unstable point merge and disappear. When  $|\kappa| > \kappa_c$  (Fig. 10c), only one fixed point remains in the phase portrait.

#### 4.4.7 Bifurcation diagram (d)

In the case  $\alpha = 0$ ,  $\beta < 1$  the bifurcation diagram consists of the curve  $\sigma_{\pi/2}$ , which corresponds to rolling along the ellipsoid's equator, and of two isolated fixed points  $\sigma_0$  and  $\sigma_\pi$ , which lie on the same level set of the integrals.

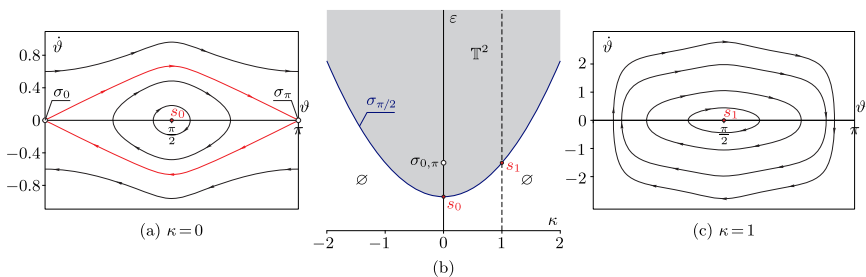


Figure 11: Bifurcation diagram (b) and examples of phase portraits (a), (c) corresponding to different values of the integral  $\kappa$  for  $\alpha = 0$ ,  $\beta = 0.5$ .

The phase portrait has, for any value of the integral  $\kappa$ , a fixed point for  $\vartheta = \pi/2$ , and is symmetric about this point. For  $\beta < 1$ , two qualitatively different types of phase portrait are possible (see Fig. 11). When  $\kappa = 0$ , the phase plane has three fixed points: two unstable ones,  $\sigma_0$  and  $\sigma_\pi$ , and a stable fixed point,  $s_0$  (which belongs to the family  $\sigma_{\pi/2}$ ). When  $\kappa > 0$ , only one stable fixed point,  $s_1$ , which belongs to the family  $\sigma_{\pi/2}$ , remains in the phase portrait.

#### 4.4.8 Bifurcation diagram (e)

When  $\beta = 1$  (with constant  $\alpha = 0$ ), the fixed points  $\sigma_0$  and  $\sigma_\pi$  corresponding to the vertical positions of the ellipsoid descend to the bifurcation curve  $\sigma_{\pi/2}$  and give rise to bifurcation branches  $\sigma_{s_0}$  and  $\sigma_{s_\pi}$ , respectively. In this case, they become stable and cease to be isolated (see Fig. 12). unstable for  $\kappa = 0$ .

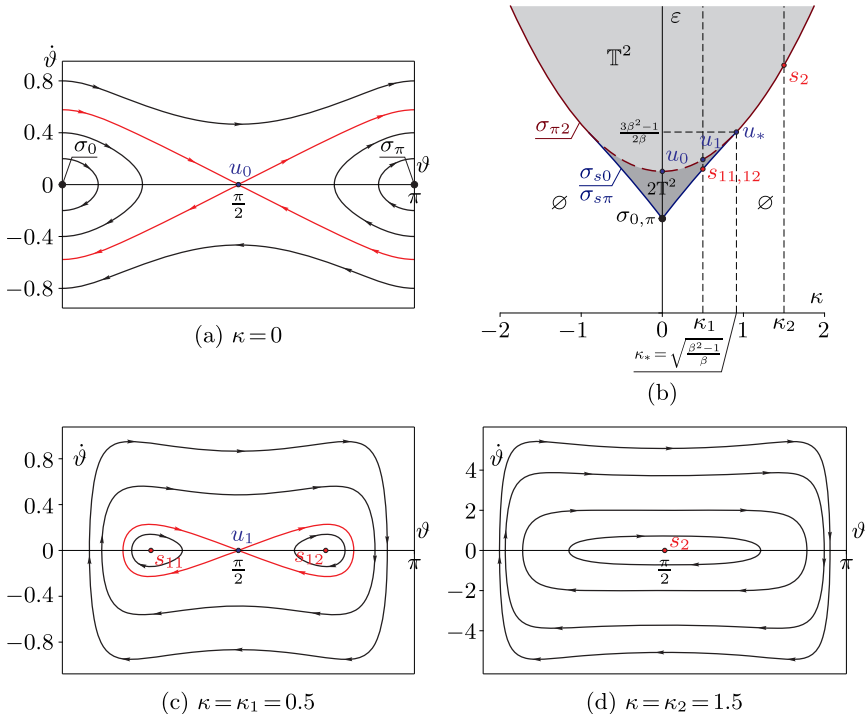


Figure 12: Bifurcation diagram (b) and examples of phase portraits (a), (c), (d) corresponding to different values of the integral  $\kappa$  for  $\alpha = 0$ ,  $\beta = 1.5$ .

When  $\kappa = 0$ , the phase portrait has three fixed points: two stable ones,  $\sigma_0$  and  $\sigma_\pi$ , and an unstable one,  $u_0$ , at  $\vartheta = \pi/2$ .

When  $0 < |\kappa| < \kappa_c$ , the phase portrait has three fixed points: two stable ones and an unstable one. Next, when  $|\kappa| = \kappa_c$ , a pitch-fork bifurcation occurs, such that the three fixed points merge into a stable fixed point<sup>2</sup>. As a result, when  $|\kappa| > \kappa_c$ , only one stable point ( $\vartheta = \pi/2$ ) remains in the phase portrait.

<sup>2</sup>We do not present here the phase portrait at the moment of bifurcation for  $\kappa = \kappa_c$  since visually it does not differ from the case  $\kappa > \kappa_c$ .

## 5 Analysis of the trajectories of an ellipsoid

In this section, we analyze how an ellipsoid behaves during motion on a plane, depending on the initial conditions and parameters of the problem, that is, to what motions of the ellipsoid the periodic trajectories of the reduced system (10) correspond.

We have already ascertained that permanent rotations correspond to the rolling motion of the ellipsoid (both its center of mass and the point of contact) in a circle. In the limiting cases when  $\vartheta = 0$  or  $\vartheta = \pi$ , the circle degenerates to a point, and as  $\vartheta \rightarrow \pi/2$ , it degenerates to a straight line. Let us find characteristic trajectories of the ellipsoid for other solutions.

In Section 2.4 we have obtained the system with one degree of freedom (10), which admits an energy integral. In the general position case, the solution of this system is periodic motion with frequency  $\omega_\vartheta$  along closed trajectories. From the expressions for the quadrature of the angle  $\psi$  (17) it follows that the function  $\dot{\psi}$  is also periodic with the same frequency  $\omega_\vartheta$ . Following our previous work [56, 57], we represent the right-hand side of the quadrature for angle  $\psi$  (17) as a Fourier series expansion

$$\dot{\psi} = \omega_\psi + \sum_{n \in \mathbb{Z} \setminus \{0\}} \Psi_n e^{in\omega_\vartheta t}, \quad (27)$$

where  $\Psi_n$  are the coefficients of Fourier series expansion,  $i$  is an imaginary unit, and  $\omega_\psi$  is the zeroth term of the expansion which is calculated by the formula

$$\omega_\psi = \frac{1}{T_\vartheta} \int_0^{T_\vartheta} \dot{\psi}(t) dt, \quad T_\vartheta = \frac{2\pi}{\omega_\vartheta}.$$

Integrating the expression (27) over time, we can represent the expression for  $\psi(t)$  as

$$\psi(t) = \omega_\psi t + \psi_\vartheta(t), \quad \psi_\vartheta(t) = \sum_{n \in \mathbb{Z} \setminus \{0\}} \frac{\Psi_n}{in\omega_\vartheta} e^{in\omega_\vartheta t}. \quad (28)$$

Here  $\psi_\vartheta(t)$  is also a periodic function with frequency  $\omega_\vartheta$ .

Next, we analyze the trajectory of the center of mass of the ellipsoid. We introduce the complex variable  $\zeta = x_c + iy_c$ , where  $x_c$  and  $y_c$  are the coordinates of the center of mass of the ellipsoid. Using (1), we can write the equation for changing the variable  $\zeta$  in the form

$$\dot{\zeta} = \frac{\kappa}{J(\vartheta) \sin \vartheta} (Z(\vartheta) + \alpha \cos \vartheta) e^{i\psi(t)}.$$

In view of (28) and the Fourier series expansion of  $\dot{\zeta}$ , the expression for  $\zeta$  has the form

$$\zeta = \zeta(0) + \sum_{n \in \mathbb{Z}} \frac{v_n}{i(\omega_\psi + n\omega_\vartheta)} e^{i(\omega_\psi + n\omega_\vartheta)t},$$

where  $v_n$  are the coefficients of the Fourier series expansion of  $\dot{\zeta}$ . Thus, in the general case the trajectory of the center of mass of the ellipsoid is a bounded curve except for the cases where the resonance relation  $\omega_\psi + n\omega_\vartheta = 0$  is satisfied.

Next, we introduce the concept of rotation number  $N$  as a ratio between frequencies  $\omega_\psi$  and  $\omega_\vartheta$

$$N = -\frac{\omega_\psi}{\omega_\vartheta} = -\frac{1}{2\pi} \int_0^{T_\vartheta} \dot{\psi}(t) dt.$$

The value of the rotation number determines the type of trajectory of the ellipsoid in absolute space. To each trajectory of the system (10) there corresponds its own rotation number depending on the values of frequencies  $\omega_\vartheta$  and  $\omega_\psi$ . The frequencies  $\omega_\psi$  and  $\omega_\vartheta$ , in their turn, are uniquely defined by the values of the first integrals  $\kappa$ ,  $\varepsilon$  and by the connectedness component of the integral manifold  $\mathcal{M}_{\kappa, \varepsilon}$ , on which the trajectory lies. Thus, the rotation number  $N$  can be defined as a function given in the (many-sheeted) bifurcation diagram. Hence, the type of trajectory of the ellipsoid in absolute space is uniquely (up to the chosen sheet) defined by the values of the first integrals  $\kappa$  and  $\varepsilon$ .

We now turn to the question of possible types of trajectories of the ellipsoid depending on  $\kappa$  and  $\varepsilon$ .

We note that it follows from (17) that, when  $\kappa = 0$ , one has  $N = 0$  for any parameter values and initial conditions. As a result, the integral manifolds  $\mathcal{M}_{0, \varepsilon}$  are completely filled by periodic solutions, i.e., they are families of resonant tori. The motions on these tori can be of two types. For small energies  $\varepsilon < \varepsilon_{\min}$  they are oscillatory motions near an equilibrium position. For large energies  $\varepsilon > \varepsilon_{\min}$  the ellipsoid rolls to infinity along the meridian crossing both of its vertices. The value of energy  $\varepsilon_{\min}$  is determined from the condition

$$\varepsilon_{\min} = \begin{cases} \varepsilon|_{\sigma_0} = 1 + \alpha & \text{for } \beta^2 < 1 + \alpha, \\ \varepsilon|_{\sigma_u, \kappa=0} = \sqrt{\frac{1 + \alpha^2 - \beta^2}{1 - \beta^2}} \beta & \text{for } \beta^2 > 1 + \alpha. \end{cases}$$

The critical invariant manifolds corresponding to the intersection of  $\kappa = 0$  with bifurcation curves are filled by inclined equilibrium positions (18) and, in the case of instability, by trajectories asymptotic to them.

Analyzing the resulting dependences, we can formulate the following proposition as a conclusion from the above reasoning (see also [58, 59]).

**Proposition.** *The trajectory of the center of mass of the ellipsoid of revolution on a plane can be of one of the following types:*

1. **a point** in the case of equilibrium positions  $\sigma_0$ ,  $\sigma_\pi$  and an inclined equilibrium position for  $\kappa = 0$ ,  $\varepsilon = U(\vartheta_*)$ .
2. **a circle** in the case of permanent rotations (15) with a constant inclination angle  $\vartheta_0 = \text{const}$  (see Fig. 3).
3. **an unbounded straight line** in the case of permanent rotations  $\sigma_{\pi/2}$  for  $\alpha = 0$  or in the case of rolling along the meridian for  $\kappa = 0$  and  $\varepsilon > \varepsilon_{\min}$ .
4. **a straight-line segment** in the case of pendulum motions near an equilibrium position along the meridian for  $\kappa = 0$  and  $\varepsilon < \varepsilon_{\min}$  and in the case of trajectories asymptotic to unstable equilibrium positions.
5. **a trajectory going to infinity without bound** for integer rotation numbers  $N \in \mathbb{Z}$  (see Fig. 13).
6. **a closed periodic trajectory** for fractionally rational rotation numbers  $N \in \mathbb{Q} \setminus \mathbb{Z}$  (see Fig. 14a).
7. **a bounded quasi-periodic curve** for all other trajectories of the system (10), except for singular trajectories asymptotic to unstable fixed points (separatrices) (see Fig. 14b).
8. **a bounded curve asymptotically tending in forward and backward time to two circles**; these trajectories of the ellipsoid correspond to the trajectories of the reduced system (10) which are asymptotic to unstable permanent rotations  $\sigma_u$ .
9. **an unbounded curve asymptotically tending in forward and backward time to two straight lines**; these trajectories of the ellipsoid correspond to the trajectories of the reduced system (10) which are asymptotic to unstable equilibrium positions  $\sigma_0$ .

Since the rotation number  $N$  depends on the values of the first integrals  $\kappa$  and  $\varepsilon$ , the conditions of resonance define some resonance curves on the plane of first integrals  $(\kappa, \varepsilon)$ . Examples of such curves for a symmetrically truncated sphere with a displaced center of mass were constructed in [57].

Figure 13 shows an enlarged fragment of the bifurcation diagram for  $\alpha = 0.5$  and  $\beta = 3$  (see Fig. 7c). The light blue curve corresponding to the resonance  $N = 0$  lies near the curve  $\sigma_u$  and “goes round the curve” as it were. But since the lower part of the curve runs very close to  $\sigma_u$ , it seems — when one looks at the figure — as if they coincide. Higher-order resonances  $N > 0$  lie still closer to  $\sigma_u$ , and so we do not represent them here. Also, Fig. 13 shows the trajectory of the center of mass of the ellipsoid (the dark red solid curve in the left part of Fig. 13) and of its point of contact (dotted dark blue curve) for the initial conditions, which correspond to the resonance  $N = 0$ . It can be seen that, for these initial conditions, the ellipsoid does not, on average, drift along the axis  $Oy$ , but goes to infinity along the axis  $Ox$ .

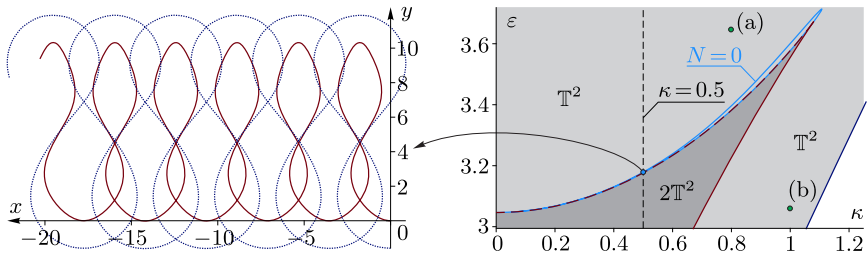


Figure 13: Right: an enlarged fragment of the bifurcation diagram (Fig. 7c,  $\alpha = 0.5$ ,  $\beta = 3$ ) with the curve corresponding to resonance  $N = 0$ . Left: the trajectory of the center of mass (solid curve) and of the point of contact (dotted curve) of the ellipsoid for the case where the resonance relation  $N = 0$  is satisfied and for  $\kappa = 0.5$ .

The numerical analysis has enabled us to find integer-valued resonances only near the curve corresponding to unstable fixed points ( $\sigma_u$ ), i.e., only for the case of diagram (c) in Fig. 7. Based on the results obtained, we can formulate the following hypothesis.

**Hypothesis.** *The trajectories of an ellipsoid of revolution on a plane are bounded for*

- $\beta^2 < 1 + \alpha$  except for the case  $\kappa = 0$  at  $\varepsilon > \varepsilon_{\min}$ ;

- $\beta^2 > 1 + \alpha$ ,  $\alpha > 0$  and  $\kappa > \kappa_{\max}$ , where  $\kappa_{\max}$  is a solution of the system

$$N(\kappa, \varepsilon) = 0, \quad \frac{\partial N}{\partial \varepsilon} = 0.$$

Figure 14 shows the trajectories of the center of mass and of the point of contact of the ellipsoid at resonance  $N = -1/7$  (Fig. 14a) and in the case of a quasi-periodic trajectory (Fig. 14b). The values of the first integrals for which these trajectories are constructed are shown in Fig. 13 as points (a) and (b), respectively. Both of these cases correspond to bounded motion of the ellipsoid on a plane.

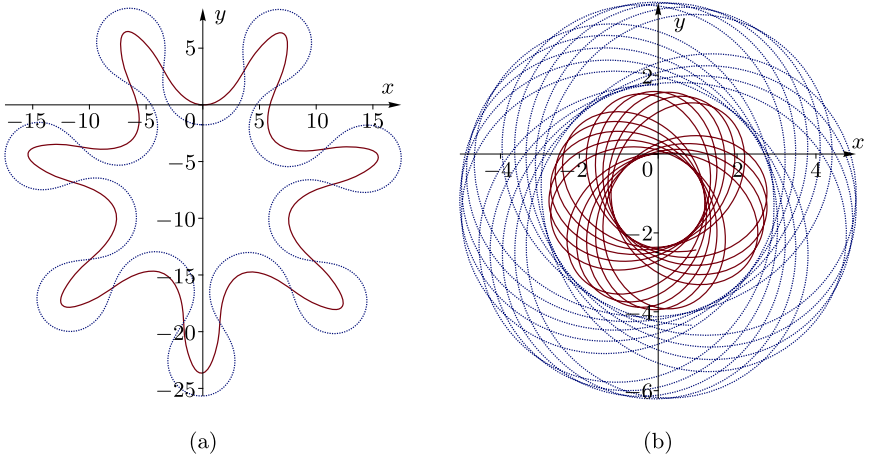


Figure 14: (a) Example of a periodic trajectory (the case  $N = -1/7$ ) for  $\kappa = 0.8$  and  $\vartheta(0) = 0.4678$ . (b) Example of a quasi-periodic trajectory for  $\kappa = 1$  and  $\vartheta(0) = 2.1$ . The solid dark red curve denotes the trajectories of the center of mass, and the dotted dark blue curve indicates the trajectories of the point of contact. Both parts of Fig. 14 are constructed for  $\alpha = 0.5$ ,  $\beta = 3$ ,  $\nu = 0.5$ ,  $\eta = 0.5$  and  $\dot{\vartheta}(0) = 0$ .

## Summary

In this work, we have carried out a complete qualitative analysis of the dynamics of an ellipsoid of revolution with a displaced center of mass on a plane with no-slip and no-spin conditions. As is well known [4, 5], the

problem of a body of revolution rolling on a plane is integrable for the above-mentioned constraints and, moreover, all integrals are represented in elementary functions. For an ellipsoid of revolution, we have found particular solutions corresponding to the rolling motion in a circle. Using these solutions, we have constructed bifurcation diagrams and performed a complete classification of these diagrams depending on the parameters of the problem.

In addition, we have shown that in the general case the motion of the ellipsoid of revolution occurs along a quasi-periodic bounded curve. However, depending on the values of the first integrals, there can also exist both unbounded and closed periodic trajectories.

A possible avenue for future research is to simulate the motion of a mobile robot of elliptic form by adding internal propulsion devices, for example, gyrostats or a pendulum/a platform or their combination. In addition, to simulate the motion of such a robot under conditions close to experimental ones, it would be interesting to add to the model irregularity of the supporting surface and/or forces and torques of rolling resistance.

## Acknowledgments

The authors thank Ivan Mamaev for useful comments and discussions.

## Funding

The work of A. Kilin (Sections 1–3) was carried out within the framework of the state assignment of the Ministry of Science and Higher Education of Russia (FEWS-2020-0009). The work of E. Pivovarova (Sections 4 and 5) is supported by the Russian Science Foundation under grant 23-71-01045.

## References

- [1] Hadamard, J., Sur les mouvements de roulement, *Mémoires de la Société des sciences physiques et naturelles de Bordeaux*, 4 sér., 1895, vol. 5, pp. 397–417.
- [2] Beghin, H., Sur les conditions d’application des équations de Lagrange à un système non holomorphe, *Bulletin de la Société Mathématique de France*, 1929, vol. 57, pp. 118–124.

- [3] Ehlers, K. and Koiller, J., Rubber rolling: Geometry and dynamics of 2-3-5 distributions, in *IUTAM Symposium on Hamiltonian Dynamics, Vortex Structures, Turbulence: Proceedings of the IUTAM Symposium held in Moscow, 25–30 August, 2006*, Springer, pp. 469–479.
- [4] Borisov, A. V. and Mamaev, I. S., Conservation laws, hierarchy of dynamics and explicit integration of nonholonomic systems, *Regular and Chaotic Dynamics*, 2008, vol. 13, no. 5, pp. 443–490.
- [5] Borisov, A. V., Mamaev, I. S., and Bizyaev, I. A., The hierarchy of dynamics of a rigid body rolling without slipping and spinning on a plane and a sphere, *Regular and Chaotic Dynamics*, 2013, vol. 18, no. 3, pp. 277–328.
- [6] Appell, P., Sur L'intégration des équations du mouvement d'un corps pesant de révolution roulant par une arête circulaire sur un plan horizontal; cas particulier du cerceau, *Rendiconti del Circolo Matematico di Palermo (1884-1940)*, 1900, vol. 14, no. 1, pp. 1–6.
- [7] Appell, P., *Traité de mécanique rationnelle*, vol. 2, Gauthier-Villars, 1904.
- [8] Chaplygin, S. A., On a motion of a heavy body of revolution on a horizontal plane, *Regular and Chaotic Dynamics*, 2002, vol. 7, no. 2, pp. 119–130.
- [9] Kilin, A. A. and Ivanova, T. B., The Integrable Problem of the Rolling Motion of a Dynamically Symmetric Spherical Top with One Nonholonomic Constraint, *Russian Journal of Nonlinear Dynamics*, 2023, vol. 19, no. 1, pp. 3–17.
- [10] Kozlov, V. V. and Kolesnikov, N. N., On theorems of dynamics, *Journal of Applied Mathematics and Mechanics*, 1978, vol. 42, no. 1, pp. 26–31.
- [11] Kilin, A. A. and Ivanova, T. B., The Problem of the Rolling Motion of a Dynamically Symmetric Spherical Top with One Nonholonomic Constraint, *Russian Journal of Nonlinear Dynamics*, 2023, vol. 19, no. 4, pp. 533–543.
- [12] Borisov, A. V. and Ivanov, A. P., A Top on a Vibrating Base: New Integrable Problem of Nonholonomic Mechanics, *Regular and Chaotic Dynamics*, 2022, vol. 27, no. 1, pp. 2–10.

- [13] Kilin, A. A. and Pivovarova, E. N., Stability of Vertical Rotations of an Axisymmetric Ellipsoid on a Vibrating Plane, *Mathematics*, 2023, vol. 11, no. 18, p. 3948.
- [14] Borisov, A. and Mamaev, I., The Rolling Motion of a Rigid Body on a Plane and a Sphere. Hierarchy of Dynamics, *Regular and Chaotic Dynamics*, 2002, vol. 7, no. 2, pp. 177–200.
- [15] Routh, E. J., *The Advanced Part of a Treatise on the Dynamics of a System of Rigid Bodies*, London: Macmillan and Co., 1892.
- [16] Borisov, A. V., Mamaev, I. S., and Kilin, A. A., The rolling motion of a ball on a surface. New integrals and hierarchy of dynamics, *Regular and Chaotic Dynamics*, 2002, vol. 7, no. 2, pp. 201–219.
- [17] Dalla Via, M., Fassò, F., and Sansonetto, N., On the dynamics of a heavy symmetric ball that rolls without sliding on a uniformly rotating surface of revolution, *Journal of Nonlinear Science*, 2022, vol. 32, no. 6, p. 84.
- [18] Fassò, F. and Sansonetto, N., On Some Aspects of the Dynamics of a Ball in a Rotating Surface of Revolution and of the Kasamawashi Art, *Regular and Chaotic Dynamics*, 2022, vol. 27, no. 4, pp. 409–423.
- [19] Borisov, A. V., Ivanova, T. B., Kilin, A. A., and Mamaev, I. S., Non-holonomic rolling of a ball on the surface of a rotating cone, *Nonlinear Dynamics*, 2019, vol. 97, no. 2, pp. 1635–1648.
- [20] Ivanova, T. B., Non-holonomic rolling of a ball on the surface of a rotating cylinder, *ZAMM-Journal of Applied Mathematics and Mechanics/Zeitschrift für Angewandte Mathematik und Mechanik*, 2020, vol. 100, no. 12, p. e202000067.
- [21] Dragović, V., Gajić, B., and Jovanović, B., Spherical and Planar Ball Bearings—Nonholonomic Systems with Invariant Measures, *Regular and Chaotic Dynamics*, 2022, vol. 27, no. 4, pp. 424–442.
- [22] Dragović, V., Gajić, B., and Jovanović, B., Spherical and Planar Ball Bearings—a Study of Integrable Cases, *Regular and Chaotic Dynamics*, 2023, vol. 28, no. 1, pp. 62–77.
- [23] Borisov, A. V., Kilin, A. A., and Mamaev, I. S., Generalized Chaplygin’s transformation and explicit integration of a system with a spherical support, *Regular and Chaotic Dynamics*, 2012, vol. 17, pp. 170–190.

- [24] Fedorov, Y. N., Motion of a rigid body in a spherical suspension, *Vestnik Moskovskogo Universiteta. Seriya 1. Matematika. Mekhanika*, 1988, , no. 5, pp. 91–93.
- [25] Cendra, H. and Etchehoury, M., Rolling of a symmetric sphere on a horizontal plane without sliding or spinning, *Reports on Mathematical Physics*, 2006, vol. 57, no. 3, pp. 367–374.
- [26] Cendra, H., Etchehoury, M., and Ferraro, S. J., Impulsive control of a symmetric ball rolling without sliding or spinning, *Journal of Geometric Mechanics*, 2010, vol. 2, no. 4, pp. 321–342.
- [27] Koiller, J. and Ehlers, K., Rubber rolling over a sphere, *Regular and Chaotic Dynamics*, 2007, vol. 12, pp. 127–152.
- [28] Bizyaev, I. A., Borisov, A. V., and Mamaev, I. S., An Invariant Measure and the Probability of a Fall in the Problem of an Inhomogeneous Disk Rolling on a Plane, *Regular and Chaotic Dynamics*, 2018, vol. 23, no. 6, pp. 665–684.
- [29] Bolsinov, A. V., Borisov, A. V., and Mamaev, I. S., Rolling of a Ball without Spinning on a Plane: The Absence of an Invariant Measure in a System with a Complete Set of Integrals, *Regular and Chaotic Dynamics*, 2012, vol. 17, pp. 571–579.
- [30] Borisov, A. V., Mamaev, I. S., and Treschev, D. V., Rolling of a rigid body without slipping and spinning: Kinematics and dynamics, *J. Appl. Nonlinear Dyn*, 2013, vol. 2, no. 2, pp. 161–173.
- [31] Kazakov, A. O., Strange attractors and mixed dynamics in the problem of an unbalanced rubber ball rolling on a plane, *Regular and Chaotic Dynamics*, 2013, vol. 18, no. 5, pp. 508–520.
- [32] Borisov, A. V., Kazakov, A. O., and Pivovarova, E. N., Regular and chaotic dynamics in the rubber model of a Chaplygin top, *Regular and Chaotic Dynamics*, 2016, vol. 21, pp. 885–901.
- [33] Mamaev, I. S. and Vetchanin, E. V., Dynamics of rubber Chaplygin sphere under periodic control, *Regular and Chaotic Dynamics*, 2020, vol. 25, pp. 215–236.
- [34] Bizyaev, I. A. and Kazakov, A. O., Integrability and stochastic behavior in some nonholonomic dynamics problems, *Russian Journal of Nonlinear Dynamics*, 2013, vol. 9, no. 2, pp. 257–265.

- [35] Ylikorpi, T., Forsman, P., Halme, A. et al., Gyroscopic precession in motion modelling of ball-shaped robots, in *Proceedings of the 28th European Conference on Modelling and Simulation, ECMS*.
- [36] Jurdjevic, V., The geometry of the plate-ball problem, *Archive for Rational Mechanics and Analysis*, 1993, vol. 124, pp. 305–328.
- [37] Bicchi, A., Prattichizzo, D., and Sastry, S. S., Planning motions of rolling surfaces, in *Proceedings of 1995 34th IEEE conference on decision and control*, vol. 3, IEEE, pp. 2812–2817.
- [38] Zheng, M., Qiang, Z., Jinkun, L., and Yao, C., Control of a spherical robot: Path following based on nonholonomic kinematics and dynamics, *Chinese Journal of Aeronautics*, 2011, vol. 24, no. 3, pp. 337–345.
- [39] Cai, Y., Zhan, Q., and Xi, X., Path tracking control of a spherical mobile robot, *Mechanism and Machine Theory*, 2012, vol. 51, pp. 58–73.
- [40] Alves, J. and Dias, J., Design and control of a spherical mobile robot, *Proceedings of the Institution of Mechanical Engineers, Part I: Journal of Systems and Control Engineering*, 2003, vol. 217, no. 6, pp. 457–467.
- [41] Zhan, Q., Cai, Y., and Yan, C., Design, analysis and experiments of an omni-directional spherical robot, in *2011 IEEE International Conference on Robotics and Automation*, IEEE, pp. 4921–4926.
- [42] Chen, W.-H., Chen, C.-P., Yu, W.-S., Lin, C.-H., and Lin, P.-C., Design and implementation of an omnidirectional spherical robot Omnicron, in *2012 IEEE/ASME International Conference on Advanced Intelligent Mechatronics (AIM)*, IEEE, pp. 719–724.
- [43] Karavaev, Y. L., Spherical robots: An up-to-date overview of designs and features, *Russian Journal of Nonlinear Dynamics*, 2022, vol. 18, no. 4, pp. 709–750.
- [44] Artemova, E. M., Karavaev, Y. L., Mamaev, I. S., and Vetchanin, E. V., Dynamics of a spherical robot with variable moments of inertia and a displaced center of mass, *Regular and Chaotic Dynamics*, 2020, vol. 25, pp. 689–706.
- [45] Marigo, A. and Bicchi, A., Rolling bodies with regular surface: Controllability theory and applications, *IEEE Transactions on Automatic Control*, 2000, vol. 45, no. 9, pp. 1586–1599.

- [46] Mukherjee, R., Minor, M. A., and Pukrushpan, J. T., Motion planning for a spherical mobile robot: Revisiting the classical ball-plate problem, *J. Dyn. Sys., Meas., Control*, 2002, vol. 124, no. 4, pp. 502–511.
- [47] García-Agúndez Blanco, A., García Vallejo, D., and Freire Macías, E., Analytical and numerical stability analysis of a toroidal wheel with nonholonomic constraints, *Nonlinear Dynamics*, 2024, vol. 112, no. 4, pp. 2453–2476.
- [48] Poincaré, H., Sur le forme nouvelle des equations de la mecanique, *C. R. Acad. Sci. Paris*, 1901, vol. 132, pp. 369–371.
- [49] Borisov, A. and Mamaev, I. S., *Rigid body dynamics, De Gruyter Studies in Mathematical Physics*, vol. 52, Walter de Gruyter GmbH & Co KG, 2018.
- [50] Bolsinov, A. V., Borisov, A. V., and Mamaev, I. S., Topology and stability of integrable systems, *Russian Mathematical Surveys*, 2010, vol. 65, no. 2, p. 259.
- [51] Bizyaev, I. A., Bolsinov, A., Borisov, A., and Mamaev, I., Topology and bifurcations in nonholonomic mechanics, *International Journal of Bifurcation and Chaos*, 2015, vol. 25, no. 10, p. 1530028.
- [52] Borisov, A. V. and Mamaev, I. S., Topological Analysis of an Integrable System Related to the Rolling of a Ball on a Sphere, *Regular and Chaotic Dynamics*, 2013, vol. 18, pp. 356–371.
- [53] Karapetyan, A., Families of permanent rotations of triaxial ellipsoid on rough horizontal plane and their branchings, *Actual Problems of Classical and Celestial Mechanics*, 1998, pp. 46–51.
- [54] Bizyaev, I. A. and Mamaev, I. S., Permanent Rotations in Nonholonomic Mechanics. Omnirotational Ellipsoid, *Regular and Chaotic Dynamics*, 2022, vol. 27, no. 6, pp. 587–612.
- [55] Markeev, A. P., The dynamics of a body contacting a rigid surface, *M.: Nauka*, 1992, p. 336.
- [56] Kilin, A. A. and Pivovarova, E. N., The rolling motion of a truncated ball without slipping and spinning on a plane, *Regular and Chaotic Dynamics*, 2017, vol. 22, no. 3, pp. 298–317.

- [57] Kilin, A. A. and Pivovarova, E. N., Qualitative Analysis of the Non-holonomic Rolling of a Rubber Wheel with Sharp Edges, *Regular and Chaotic Dynamics*, 2019, vol. 24, pp. 212–233.
- [58] Borisov, A. V., Mamaev, I. S., and Kilin, A. A., Dynamics of rolling disk, *Regular and Chaotic Dynamics*, 2003, vol. 8, no. 2, pp. 201–212.
- [59] Borisov, A. V. and Mamaev, I. S., An inhomogeneous Chaplygin sleigh, *Regular and Chaotic Dynamics*, 2017, vol. 22, pp. 435–447.

